PP6 Controls T Cell Development and Homeostasis by Negatively Regulating Distal TCR Signaling

Jian Ye, Hao Shi, Ye Shen, Chao Peng, Yan Liu, Chenyu Li, Kejing Deng, Jianguo Geng, Tian Xu, Yuan Zhuang, Biao Zheng and Wufan Tao

J Immunol 2015; 194:1654-1664; Prepublished online 21 January 2015;
doi: 10.4049/jimmunol.1401692
http://www.jimmunol.org/content/194/4/1654

The Journal of Immunology is published twice each month by
The American Association of Immunologists, Inc.,
9650 Rockville Pike, Bethesda, MD 20814-3994.

Print ISSN: 0022-1767 Online ISSN: 1550-6606.

PP6 Controls T Cell Development and Homeostasis by Negatively Regulating Distal TCR Signaling

Jian Ye,* Hao Shi,* Ye Shen,* Chao Peng,* Yan Liu,* Chenyu Li,* Kejing Deng,* Jianguo Geng,† Tian Xu,*,‡ Yuan Zhuang,*,§ Biao Zheng,¶ and Wufan Tao*

T cell development and homeostasis are both regulated by TCR signals. Protein phosphorylation and dephosphorylation, which are catalyzed by protein kinases and phosphatases, respectively, serve as important switches controlling multiple downstream pathways triggered by TCR recognition of Ags. It has been well documented that protein tyrosine phosphatases are involved in negative regulation of proximal TCR signaling. However, how TCR signals are terminated or attenuated in the distal TCR signaling pathways is largely unknown. We investigated the function of Ser/Thr protein phosphatase (PP) 6 in TCR signaling. T cell lineage-specific ablation of *PP6* in mice resulted in enhanced thymic positive and negative selection, and preferential expansion of fetal-derived, IL-17–producing Vγ6Vδ1$^+$ T cells. Both *PP6*-deficient peripheral CD4$^+$ helper and CD8$^+$ cytolytic cells could not maintain a naive state and became fast-proliferating and short-lived effector cells. *PP6* deficiency led to profound hyperactivation of multiple distal TCR signaling molecules, including MAPKs, AKT, and NF-κB. Our studies demonstrate that *PP6* acts as a critical negative regulator, not only controlling both αβ and γδ lineage development, but also maintaining naive T cell homeostasis by preventing their premature activation before Ag stimulation. ***The Journal of Immunology*****, 2015, 194: 1654–1664.**

T cell development and activation are tightly regulated by signals initiated from the TCR. The strength and duration of TCR signals depend on the TCR affinity to peptide–MHC and are further modulated by the downstream signaling molecules consisting of the proximal and distal signaling cascades (1). TCR signal strength is a critical determinant for thymic positive and negative selection, during which insufficient or excessively strong signals will lead to elimination of useless or potentially autoreactive T cells, respectively (2, 3). Upon maturation, most T cells are thought to maintain their naive state by sensing tonic TCR signals, which are necessary for survival and homeostatic proliferation without premature activation (4). During pathogenic infection, Ag-specific T cells are clonally activated by a strong TCR signal. T cell activation leads to clonal expansion of short-lived effectors and differentiation into the long-lived memory cells, which provide the host with immediate and future protection against the pathogen, respectively.

Protein phosphorylation is an important protein modification that regulates TCR signaling (1). Protein tyrosine kinases and protein Ser/Thr kinases are mostly involved in positive regulation of proximal and distal TCR signaling, respectively, and their roles in this process have been well established. Protein phosphatases (PPs) are largely responsible for negative regulation of TCR signaling. Based on their substrate specificity, PPs can be mainly classified into three subgroups: protein tyrosine phosphatases (PTPs), dual-specificity phosphatases (DUSPs), and Ser/Thr PPs. Four PTPs including PTPN2, PTPN6 (SHP-1), PTPN12 (PTP-PEST), and PTPN22 (PEP) have been demonstrated to function as key signaling modulators attenuating proximal TCR signaling during positive selection and T cell activation. CD45 (PTPRC), a special PTP, regulates proximal TCR signaling in both positive and negative manners. CD45 deficiency blocks TCR signaling and early T cell development in thymus (5). DUSPs are negative regulators of MAPKs; however, all reported DUSP-deficient mice do not exhibit any detectable defect of thymocyte development (6). The roles of PPs in regulating TCR signal cascade still remain to be investigated.

PP2A subfamily, a major class of PPs, consists of three phosphatases: PP2A, PP4, and PP6 (7). The physiological functions of *PP2A* in T cell biology have so far not been reported. PP4 can inhibit NF-κB activity by dephosphorylating IKKβ in Jurkat T cells (8). T cell–specific deletion of *PP4* in mice impaired positive selection of thymocytes and compromised Ag-specific T cell proliferation by attenuating activation of PLCγ1 and ERK (9). Until now, there were only a limited number of reports describing *PP6* functions at cellular or biochemical levels. The holoenzyme of PP6 is composed of a catalytic subunit, a SAPS domain subunit, and an ankyrin repeat subunit (10). PP6 regulates chromosome segregation in mitosis through inhibiting Aurora A

*State Key Laboratory of Genetic Engineering and Institute of Developmental Biology and Molecular Medicine, National Center for International Research of Development and Disease, School of Life Sciences, Fudan University, Shanghai 200433, China; †Department of Biologic and Materials Sciences, University of Michigan School of Dentistry, Ann Arbor, MI 48109; ‡Department of Genetics, Howard Hughes Medical Institute, Yale University School of Medicine, New Haven, CT 06536; §Department of Immunology, Duke University Medical Center, Durham, NC 27701; and ¶School of Life Sciences, East China Normal University, Shanghai 200241, China

Received for publication July 7, 2014. Accepted for publication December 15, 2014.

This work was supported by the National Basic Research Program of China (Grants 2013CB945304, 2011CB510102, and 2006CB806700), the National Natural Science Foundation of China (Grants 31171406, 81228019, and 31471380), the High-Technology Research and Development Program of China (Grant 2007AA022101), Key Projects Grant for Basic Research (Grants 08JC1400800 and 12JC1400600) from the Science and Technology Committee of Shanghai Municipality, and the 211 and 985 Projects of the Chinese Ministry of Education.

J.Y., Y.Z., and W.T. designed the research; J.Y., H.S., Y.S., C.P., Y.L., and C.L. performed research, data collection, and statistical analysis; K.D., T.X., J.G., and B.Z. contributed vital new reagents or analytical tools; J.Y., B.Z., Y.Z., and W.T. analyzed and interpreted data; and J.Y., Y.Z., B.Z., and W.T. wrote the manuscript.

Address correspondence and reprint requests to Dr. Tao Wufan or Dr. Biao Zheng, Fudan University, 220 Handan Road, Shanghai 200433, China (T.W.) or School of Life Sciences, East China Normal University, Shanghai 200241, China (B.Z.). E-mail addresses: wufan_tao@fudan.edu.cn (T.W.) or bzheng@bcm.edu (B.Z.)

The online version of this article contains supplemental material.

Abbreviations used in this article: 7AAD, 7-aminoactinomycin D; DN, double-negative; DP, double-positive; DUSP, dual-specificity phosphatase; ES, embryonic stem; FRT, Flp recombination target; PK, protein kinase; PP, protein phosphatase; PTP, protein tyrosine phosphatase; SP, single-positive; Treg, regulatory T cell; WT, wild type.

activity (11) and facilitating the repair of DNA double-strand breaks by activating DNA-activated protein kinase (DNA-PK) and dephosphorylating γ-H2AX in HeLa cells (12, 13). Involvement of *PP6* in modulating NF-κB activity is suggested by findings that the PP6 protein interacts with and protects IκBε from TNF-α–induced degradation in Cos7 cells (14). PP6 also suppresses IL-1–stimulated TAK1 activation by dephosphorylating TAK1 in 293 cells (15). Recent evidence suggests that PP6 may also regulate Hippo signaling via interaction with MOB1B (16). However, the physiological functions of PP6, especially in T cell biology, are not known.

In this study, we investigated functions of the *PP6* gene in T cells by generating and analyzing *PP6*-deficient mice. Whereas conventional deletion of *PP6* led to early embryonic lethality, T cell–specific ablation of *PP6* revealed essential regulatory roles for *PP6* in both T cell development and activation. Both positive and negative selection events are enhanced during αβ T cell development, and fetal-derived, IL-17–producing Vγ6Vδ1$^+$ T cells are preferentially expanded in *PP6$^{F/F}$;Lck-Cre* mice. In peripheral lymphoid organs, *PP6*-deficient mature T cells are no longer able to maintain their naive state and become short-lived effectors. *PP6* deficiency leads to a profound hyperactivation of multiple signaling molecules distal to the TCR. Collectively, our study demonstrates that *PP6* is a major negative regulator of TCR signals by controlling multiple downstream pathways in the distal end of the TCR signaling cascade.

Materials and Methods

Generation of PP6*-deficient mice*

To construct the *PP6* gene–targeting vector, we isolated a genomic DNA fragment containing exons 3–7 of *PP6* from the 129/Sv mouse genomic phage library (Stratagene). In the gene targeting vector, a nuclear *β-gal* reporter gene with a splicing acceptor and a neomycin expression cassette flanked by Flp recombination target (FRT) sites were inserted after exon 4. Splice acceptor was derived from exon 2 of mouse *En2* gene. A pair of LoxP sites was also inserted at SpeI and BamHI sites flanking exons 5 and 6, and a diphtheria toxin A expression cassette was used as a negative selection marker. The linearized *PP6* targeting vector was electroporated into mouse embryonic stem (ES) cells (W4/129S6 ES; Taconic Transgenic), and the recombinant ES cell clones were screened by PCR and further confirmed by Southern blot analysis. Two recombinant ES clones were injected into C57BL/6J blastocysts to produce chimera mice. *PP6$^{+/galeo}$* mice were crossed with *Act-Flpe* transgenic mice (stock no. 003800) to delete the *β-gal* and neo cassette to generate *PP6$^{+/F}$* mice. *PP6$^{+/F}$* mice were backcrossed with C57BL/6 for six generations before crossing with *Lck-Cre* (17) or *CD4-Cre* (18) transgenic mice. *PP6$^-$* null allele was generated after removal of the fragment containing exons 5 and 6 by introducing a *Cre* transgene driven by universal *Pgk* promoter or T cell–specific *Lck* or *CD4* promoter. Deletion of exons 5 and 6 led to a frame shift and multiple stop codons in exon 7 in truncated *PP6* mRNA. Oligos pp6-FRT-F1 (p1: 5′-TGTGGATTCTGGGGTTCAAAGTC-3′); PP6-loxP2-R1 (p2: 5′-CAGCACCTGACTCCATTATGTTGG-3′); and pp6-FRT-R1 (p3: 5′- GGTTCAGTTCTCAGTAGCCATAGGG-3′) were used for genotyping of *PP6^F* allele and *PP6$^-$* null allele by PCR.

Other transgenic mice

Pgk-Cre (19) transgenic mice were described previously. *Act-Flp* transgene mice and B6.SJL (stock no. 002014) mice were purchased from The Jackson Laboratory. The OT-II and OT-I TCR transgenic mice were kindly provided by Dr. Xuetao Cao. Mice at 6–10 wk old were used for experiments unless otherwise noted. Bone marrow chimeras were generated by i.v. transfer of T cell–depleted bone marrow into sublethally irradiated B6.SJL mice as described previously (20). All mice were kept in specific pathogen-free conditions, and animal-related procedures were approved by the Animal Care and Use Committee of the Institute of Developmental Biology and Molecular Medicine at Fudan University.

Immunoblot, flow cytometry, and cell sorting

T cells were stimulated with 100 ng/ml PMA plus 1 μM ionomycin or soluble anti-CD3ε plus anti-CD28 or anti-CD4 (10 μg/ml each) for various times before being lysed with radioimmunoprecipitation assay buffer containing 1 mM PMSF and 1× proteinase inhibitor (Roche). Immunoblots were performed as described previously (21) with Abs to p-ERK (4370), ERK (4695, 9107), p-JNK (4668), JNK (9258), p-p38 (4511), p38 (8690), p-c-Raf (9427), p-MEK1/2 (9154), p-MEK4 (9156), p-MEK3/6 (9231), MEK1/2 (9126), p-IKKα/β (2697), IKKα (2682), p-p65 (8242), p65 (3033), p-IκBα (2859), IκBα (4814), p-IκBε (4924), IκBε (9249), p-Zap70 (2717), Zap70 (3165), p-LAT (3584), LAT (9166), p-LCK (2751), LCK (2787), p-PLCγ1 (2821), and PLCγ1 (5690) purchased from Cell Signaling. Anti-PP6 (07-1224) was from Millipore, and anti–β-Actin (AC-15) was from Sigma-Aldrich. Images were acquired with Tanon-5200 or Biorad ChemiDoc MP System, and the density of the bands was quantified by ImageJ.

For surface marker analysis, cells were stained with indicated Abs in PBS containing 2% FBS. Intracellular staining was performed according to the manufacturer's instructions. Abs to Bcl-2 (3F11), CD4 (RM4-5), CD8b (H35-17.2), CD3ε (145-2C11), TCRβ (H57-597), TCRγδ (GL3), CD5 (53–7.3), CD24 (30-F1), CD69 (H1.2F3), CD25 (PC61.5), CD44 (1M7), CD62L (MEL-14), CD45.1 (A20), CD45.2 (104), TCRVβ5 (MR9–4), TCRVβ8 (KJ16), TCRVβ11 (C21), TCRVα2 (B20.1), IL-7R (SB/199), TCRVγ1 (2.11), TCRVγ4 (UC3-10A6), TCRVγ5 (536), CCR6 (140706), CD27 ((LG.7F9), IFN-γ (XMG1.2), IL-4 (11B11), IL-17 (TC11-18H10), Foxp3, and Ki67 Kit were purchased from BD or eBioscience. Anti-TCR Vγ6 was a gift from Dr. Robert E. Tigelaar at Yale University. The staining of Vγ6$^+$ γδ T cells has been described previously (22). Dead cells were excluded during analysis according to their light-scattering characteristics and/or 7-aminoactinomycin D (7AAD) staining.

For staining of mitochondria, lymphocytes were incubated with 20 nM MitoTracker Green (Invitrogen) at 37°C for 20 min. Reactive oxygen species were measured by incubation with 10 μM dihydroethidium (Sigma-Aldrich) at 37°C for 30 min. CFSE labeling was performed by incubating sorted cells with 5 μM CFSE (Invitrogen) at 37°C for 20 min followed by adoptive transfer into B6.SJL mice. Flow cytometry data were acquired on FACSCalibur or LSRII (BD) and were analyzed with FlowJo software (Tree Star). CD4$^+$ T cells were isolated from splenocytes with anti-CD4–coated magnetic microbeads (Miltenyi Biotec). γδ T cells were sorted on FACSAria II (BD Biosciences).

Adoptive transfer

For adoptive transfer, freshly isolated splenocytes containing an equal amount of wild type (WT) or *PP6*-deficient CD4$^+$ T cells or CFSE-labeled purified CD4$^+$ T cells were i.v. injected into B6.SJL as described previously (23).

X-gal staining

PP6$^{+/galeo}$ mice were used for X-gal staining to determine the expression pattern of *PP6*. Tissue processing, frozen section, X-gal staining, and immunofluorescent microscopic analysis were performed as described previously (24).

Quantitative RT-PCR

Total RNA was isolated from T cells using the RNeasy Mini Kit (Qiagen), and first-strand cDNA was synthesized using the Sensiscript Reverse Transcription Kit (Qiagen). The abundance of mRNA for each gene was determined by real-time quantitative PCR using SYBR Green master mix (Applied Biosystems) in Prism 7500 (Applied Biosystems). A pair of primers specific for *PP6* was separately located in exons 5 and 6. Primer sequences will be provided upon request. Expression values were calculated using the $2^{-\Delta Ct}$ method with *Actinb* as an endogenous control.

BrdU incorporation assay

Mice were i.p. (for adults) or s.c. (for neonates) injected with 50 mg/kg BrdU two times with a 2-h interval. The thymus and spleen were taken 24 h after the first injection. Cells were first stained with surface markers, then fixed and stained with a BrdU staining kit (BD) followed by FACS analysis.

Calcium flux

Calcium flux was measured using the Fluo-4 Direct Calcium Assay Kit (Invitrogen). In brief, 2 × 10^7 thymocytes were resuspended in 500 μl Fluo-4 Direct calcium reagent with 6 μM Fura Red and incubated at 37°C for 30 min. After washing, the cells were labeled with anti–CD4-PerCy7 and anti–CD8-allophycocyanin for 15 min on ice followed by a 30-min incubation at room temperature. Calcium influx was analyzed by FACS. After measurement of baseline levels for 30 s, anti-CD3 and anti-CD28

plus anti-Armenian hamster IgG (eBioscience) as cross-linking Ab were added. Events were collected for a total time of 10 min.

Statistics analysis

Statistical analysis was conducted using an unpaired *t* test by GraphPad Prism. The *p* values <0.05 were considered significant.

Results

Essential role of PP6 in embryonic development

We first generated a *PP6* mutant allele, $PP6^{galeo}$, in mouse ES cells (Supplemental Fig. 1A, 1B) using a "conventional first, conditional ready" gene-targeting strategy (25). RT-PCR analysis indicated that $PP6^{galeo}$ allele is a hypomorphic allele (Supplemental Fig. 1C). In $PP6^{galeo}$ allele, the expression of *β-gal* reporter is under the control of the endogenous *PP6* promoter, and β-galactosidase is in-frame fused with the first 78 aa of the PP6 protein after splicing. This knocked-in β-galactosidase reporter revealed that *PP6* was highly expressed in the brain and testis (Supplemental Fig. 1G). When $PP6^{+/galeo}$ mice were intercrossed, $PP6^{galeo/galeo}$ embryos were recovered with the expected ratio at embryonic day 10, frequently lost at embryonic day 14.5, with remaining ones occasionally exhibiting exencephaly (Supplemental Fig. 1D and data not shown), and rarely found after birth (at postnatal day 10 WT:HET:HO = 103:159:3). The $PP6^{F}$ conditional allele was generated after removing the β-*gal* reporter gene and neomycin expression cassettes with Flp/FRT-mediated recombination (Supplemental Fig. 1A). $PP6^{F/F}$ mice were phenotypically indistinguishable from WT littermates and used as controls in the studies described later. Germline deletion of the $PP6^{F}$ allele with *Pgk-Cre* resulted in lethality at early embryonic stages (Supplemental Fig. 1H), confirming the critical function of *PP6* in embryonic development.

Abnormal thymocyte development in $PP6^{F/F}$;Lck-Cre mice

To study the function of *PP6* in T cells, we crossed the $PP6^{F}$ allele into *Lck-Cre* mice to produce $PP6^{F/F}$;*Lck-Cre* mice. Genomic PCR and Western blot analyses showed that *PP6* was deleted efficiently in the thymocytes of $PP6^{F/F}$;*Lck-Cre* mice (Supplemental Fig. 1E, 1F). T cell–specific ablation of *PP6* resulted in abnormal thymocyte development. Both proportion and numbers of CD4 single-positive (SP) cells, CD8 SP cells, and $CD4^{+}CD8^{+}$ (double-positive [DP]) cells, as well as numbers of total thymocytes, were significantly reduced in $PP6^{F/F}$;*Lck-Cre* mice (Fig. 1A). In contrast, the proportion and number of $CD4^{-}CD8^{-}$ (double-negative [DN]) cells were increased in the mice. However, further analyses revealed that DN subpopulations of $PP6^{F/F}$;*Lck-Cre* thymocytes appeared normal after removing γδ T cells (Fig. 1C), indicating that the increase of γδ T cells should be the reason for an apparent upsurge of DN thymocytes in $PP6^{F/F}$;*Lck-Cre* mice (see *Increased IL-17–producing γδ T cells in $PP6^{F/F}$;Lck-Cre mice*). The $PP6^{F/F}$;*Lck-Cre* mice had considerably fewer peripheral T cells (7–12% that of the control; Fig. 1B and Supplemental Fig. 2A). Numbers of regulatory T cells (Tregs) were also decreased in the thymus and periphery of $PP6^{F/F}$;*Lck-Cre* mice (Fig. 1D). Although the proportion of peripheral Tregs increased in adult $PP6^{F/F}$;*Lck-Cre* mice, it is still significantly lower in the 1-wk-old mice (Fig. 1D, 1E, and Supplemental Fig. 2B, 2C). These data indicate that *PP6* plays important roles in T cell development.

Effects of PP6 deficiency on thymic positive and negative selection

The effects of *PP6* deficiency on thymocyte development were further examined with the maturation and activation markers: CD5, CD24, and CD69. CD5 expression at the DP stage is proportional to TCR signaling strength during positive selection (26), whereas CD69 upregulation in DP cells is indicative of positive selection in response to TCR signaling (27). CD5 expression was increased in *PP6*-deficient DP cells, and CD69 expression was elevated in both mutant DP and SP cells (Fig. 2A). CD24 expression in SP cells decreases upon their maturation (28). We found that the proportion of $CD24^{lo}$ SP thymocytes was increased in the $PP6^{F/F}$;*Lck-Cre* mice (Fig. 2A). Collectively, these observations suggest that *PP6* deficiency may promote positive selection and enhance thymocyte maturation.

To further examine the effect of *PP6* deficiency on thymocyte positive selection and to overcome the difficulty of evaluating thymocyte selection in mice with a diverse T cell repertoire, we introduced MHC-II–restricted OT-II or MHC-I–restricted OT-I TCR transgenes into $PP6^{F/F}$;*Lck-Cre* mice to test MHC class II and class I–mediated positive selection, respectively. Thymocytes

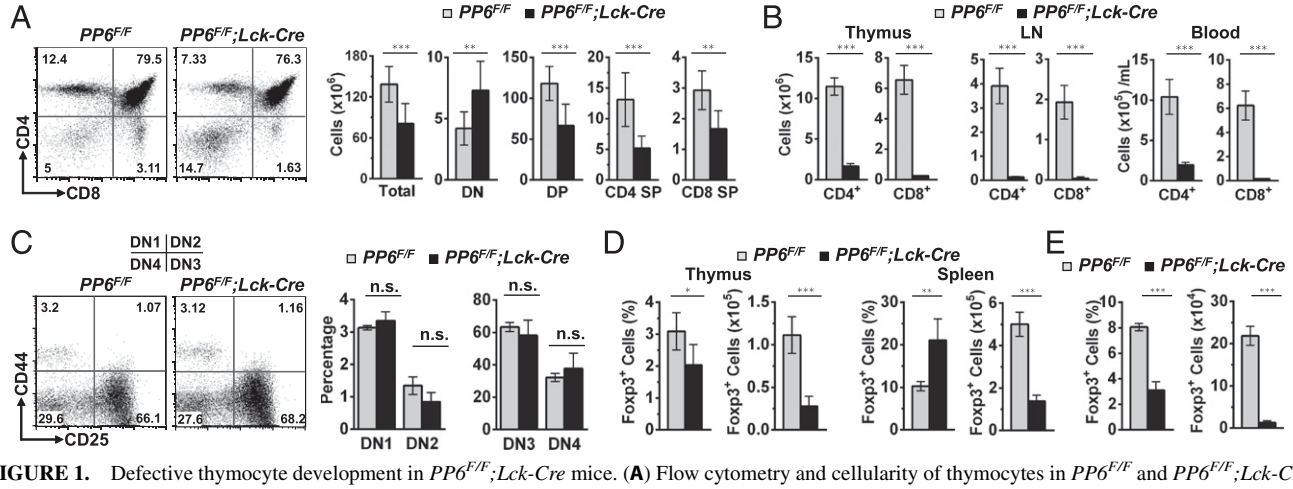

FIGURE 1. Defective thymocyte development in $PP6^{F/F}$;*Lck-Cre* mice. (**A**) Flow cytometry and cellularity of thymocytes in $PP6^{F/F}$ and $PP6^{F/F}$;*Lck-Cre* mice. Numbers in quadrants (*left panel*) indicate percent cells in each. $n = 8$ for each genotype. (**B**) Cellularity of $CD4^{+}$ and $CD8^{+}$ lymphocytes from spleen, lymph node (LN), and blood of $PP6^{F/F}$ and $PP6^{F/F}$;*Lck-Cre* mice. $n = 8$ for each genotype. (**C**) Flow cytometry of thymocytes gated on DN cells ($CD4^{-}$ $CD8^{-}$ $TCR\gamma\delta^{-}$ $CD11b^{-}$ $NK1.1^{-}B220^{-}$) and frequency of DN thymocyte subpopulations from $PP6^{F/F}$ and $PP6^{F/F}$;*Lck-Cre* mice. Numbers in quadrants (*left panel*) indicate percent cells in each. $n = 4$ for each genotype. (**D** and **E**) Percentage and cellularity of Tregs gated on CD4 SP thymocytes (D, *left panels*) or $CD4^{+}$ splenocytes (D, *right panels*) from adult $PP6^{F/F}$ and $PP6^{F/F}$;*Lck-Cre* mice or $CD4^{+}$ T cells of LNs from 1-wk-old $PP6^{F/F}$ and $PP6^{F/F}$;*Lck-Cre* mice (E). $n = 4$ for each genotype. Data shown are representative from at least three (A, B, D, and E) and two (C) independent experiments. Data are presented as mean ± SD. $^{*}p < 0.05$, $^{**}p < 0.01$, $^{***}p < 0.001$. n.s., not significant.

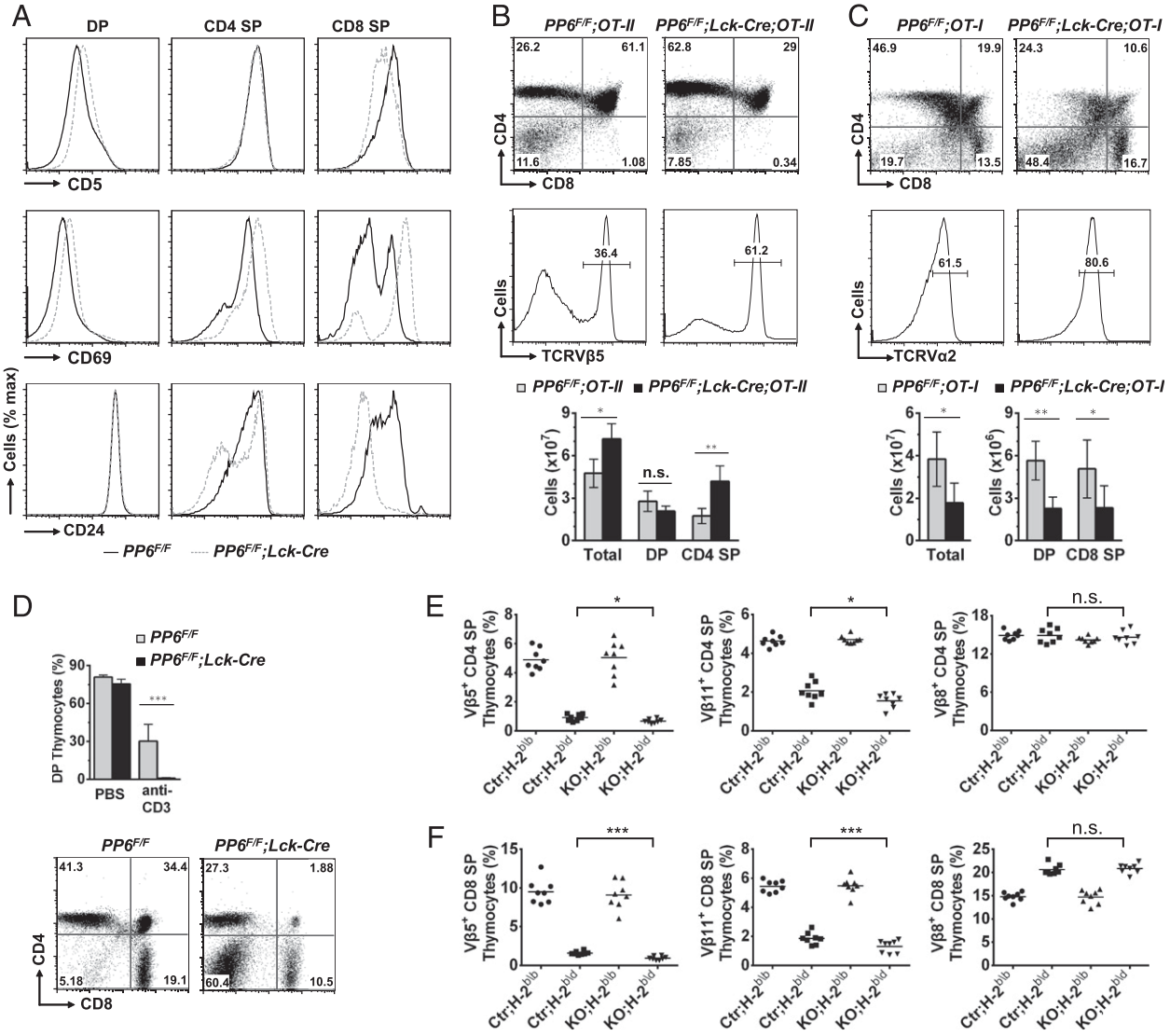

FIGURE 2. Enhanced positive and negative selection in *PP6*-deficient mice. (**A**) Surface expression of CD5, CD24, and CD69 on *PP6*-deficient and control thymocytes gated as indicated. $n \geq 4$ for each genotype. (**B**) Flow cytometry (*top panel*) and cellularity (*bottom panel*) of thymocytes in $PP6^{F/F}$;*OT-II* and $PP6^{F/F}$;*Lck-Cre;OT-II* mice. Numbers in quadrants (*top panel*) indicate percent cells in each. (*Middle panel*) Staining with Ab to the OT-II–specific V region Vβ5. $n = 5$ for each genotype. (**C**) Flow cytometry (*top panel*) and cellularity (*bottom panel*) of thymocytes in $PP6^{F/F}$;*OT-I* and $PP6^{F/F}$;*Lck-Cre;OT-I* mice. Numbers in quadrants (*top panel*) indicate percent cells in each. (*Middle panel*) Staining with Ab to the OT-I–specific V region Vα2. $n = 4$ for each genotype. (**D**) Flow cytometry of thymocytes and percentage of DP thymocytes of $P6^{F/F}$ and $PP6^{F/F}$;*Lck-Cre* mice 48 h after administration of 10 μg anti-CD3 mAb or PBS. $n = 4$ for each genotype. (**E** and **F**) Statistical analysis of the percentage of $V\beta5^+$, $V\beta11^+$, and $V\beta8^+$ thymocytes gated on CD4 SP (E) or CD8 SP (F) in $PP6^{F/F}$ (Ctr) and $PP6^{F/F}$;*Lck-Cre* (KO) mice with ($H\text{-}2^{b/d}$) or without ($H\text{-}2^{b/b}$) expression of MHC molecule I-E^d. Deletion of $V\beta5^+$ and $V\beta11^+$ cells by superantigen only occurs on $H\text{-}2^{b/d}$, but not $H\text{-}2^{b/b}$ backgrounds. $V\beta8^+$ cells are not affected. Each symbol represents a single mouse; small horizontal lines indicate the mean. Data shown are representative from two independent experiments. (B and D) Data are presented as mean ± SD. $^*p < 0.05$, $^{**}p < 0.01$, $^{***}p < 0.001$. n.s., not significant.

expressing the OT-II TCR are positively selected along the CD4 lineage (29). FACS analysis showed that the proportion and numbers of total CD4 SP cells, OT-II–specific $TCRV\beta5^+$ thymocytes, and $CD69^{hi}$ and $CD24^{lo}$ CD4 SP cells were increased in $PP6^{F/F}$;*Lck-Cre;OT-II* mice in comparison with the control mice (Fig. 3B and Supplemental Fig. 2D). These results suggest that *PP6* deficiency enhances positive selection of the MHC-II–restricted thymocytes. OT-I TCR–expressing $CD8^+$ thymocytes are favored for positive selection in OT-I transgenic mice (30). In OT-I mice, *PP6* deficiency resulted in an increase of proportion of $CD69^{hi}$ DP and CD8 SP cells (Supplemental Fig. 2E), indicating enhancement of positive selection of $PP6^{F/F}$;*Lck-Cre;OT-I* thymocytes. In *OT-I* mice, *PP6* ablation also led to a higher proportion of $TCRV\alpha2^{hi}$ and $CD24^{lo}$ CD8 SP cells (Fig. 2C, *middle panels*, and Supplemental Fig. 2E) and a higher ratio between post selected OT-I–specific $TCRV\alpha2^{hi}$ CD8 SP cells and the preselection stage cells, including DP and the CD4 transitional thymocytes (31) (Supplemental Fig. 2F), implying that more CD8 SP cells become phenotypically mature cells. However, an overall reduction of total thymocyte, DP, and CD8 SP thymocytes was also observed (Fig. 2C, *bottom panels*). All these observations are consistent with the previously described behavior of the OT-I thymocytes expressing a constitutive NF-κB. Enhancement of OT-I signals by constitutive activation of NF-κB pushed a portion of positive selecting thymocytes into negative selection, a phenomenon called *pseudonegative selection* (32).

Thymocytes bearing high-affinity TCRs for self-Ags undergo clonal deletion or negative selection. To investigate whether *PP6* is

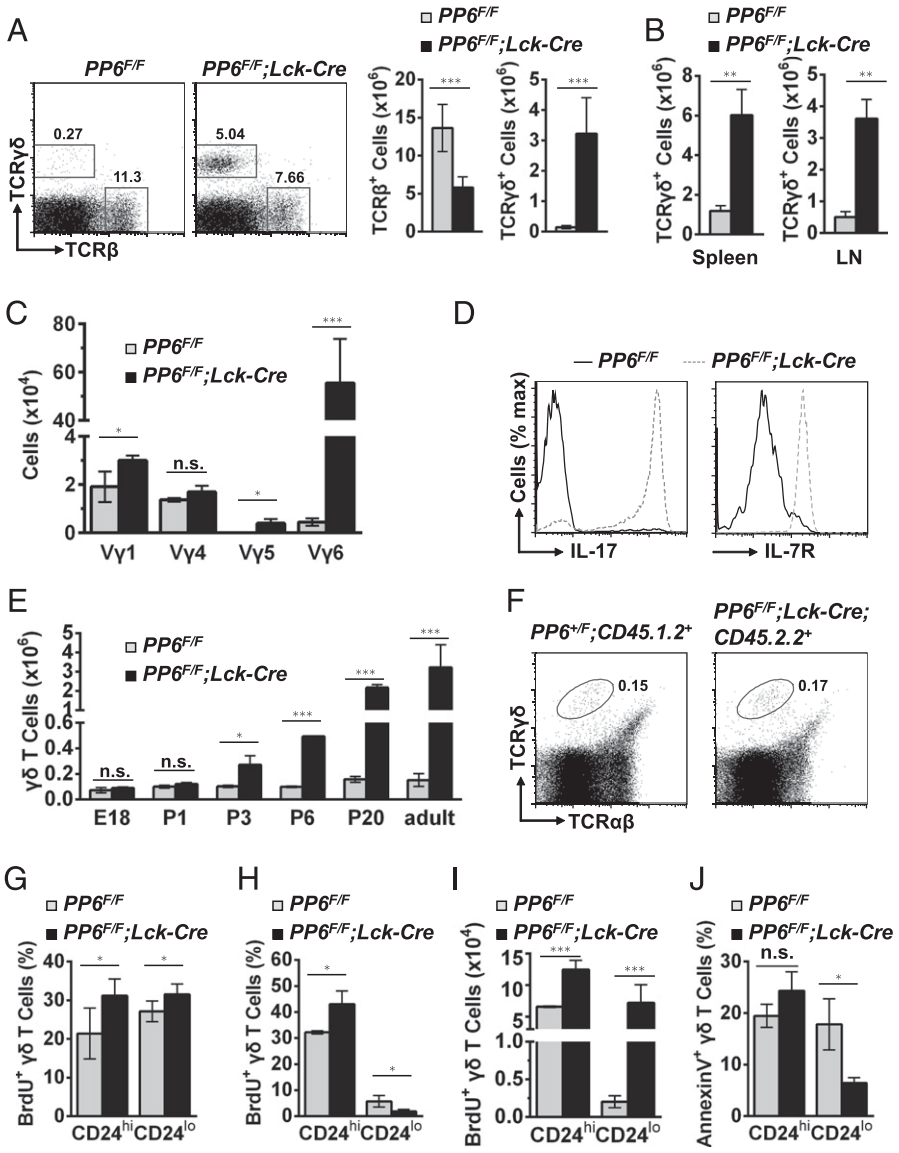

FIGURE 3. Increased IL-17–producing Vγ6Vδ1$^+$ T cells in *PP6$^{F/F}$;Lck-Cre* mice. (**A**) Flow cytometry and cellularity of αβ and γδ T cells in the thymus with indicated genotype. $n = 5$ for each genotype. (**B**) Cellularity of γδ T cells in spleen and lymph node (LN) from *PP6$^{F/F}$* and *PP6$^{F/F}$;Lck-Cre* mice. $n = 5$ for each genotype. (**C**) Cellularity of Vγ1$^+$, Vγ4$^+$, Vγ5$^+$, and Vγ6$^+$ γδ T cells from thymus in *PP6$^{F/F}$* and *PP6$^{F/F}$;Lck-Cre* mice. $n = 4$ for each genotype. (**D**) FACS analysis of intracellular expression of IL-17 and surface expression of IL-7R of γδ T thymocytes, with indicated genotypes. (**E**) The cellularity of γδ T cells in the thymus from fetal or postnatal *PP6$^{F/F}$* and *PP6$^{F/F}$;Lck-Cre* mice. $n \geq 3$ for each genotype at indicated ages. (**F**) Flow cytometry analysis of thymus of B6.SJL recipient mice transplanted with a mixture of equal number of bone marrow cells from *PP6$^{F/+}$; CD45.1.2$^+$* or *PP6$^{F/F}$;Lck-Cre;CD45.2.2$^+$* mice. Numbers adjacent to outlined areas indicate the γδ T cell percentage of the gated CD45.1.2$^+$ or CD45.2.2$^+$ thymocytes. $n = 4$ for each genotype. (**G**) Percentage of BrdU$^+$ γδ T cells from *PP6$^{F/F}$* and *PP6$^{F/F}$;Lck-Cre* mice at P2, which were injected s.c. with BrdU 24 h before sacrificed for flow cytometry. $n = 4$ for each genotype. (**H** and **J**) Proliferation and apoptosis of CD24^{hi} and CD24^{lo} γδ thymocytes from adult mice (6–8 wk) with indicated genotypes were evaluated flow cytometrically by measuring BrdU incorporation (H) or Annexin V staining (J), respectively. $n = 3$ for each genotype. (**I**) Number of BrdU$^+$ CD24^{hi} and BrdU$^+$ CD24^{lo} γδ T cells in thymus from adult mice (6–8 wk) with indicated genotypes. $n = 4$ for each genotype. Data shown are representative from two (C and F) or three (A and D) independent experiments. (A–C, E, and G–J) Data are presented as mean ± SD. $^*p < 0.05$, $^{**}p < 0.01$, $^{***}p < 0.001$. n.s., not significant.

required for clonal deletion, *PP6$^{F/F}$;Lck-Cre* or control mice were injected with the CD3 Ab to mimic high-affinity TCR signals. Under the experimental condition, DP thymocytes in *PP6$^{F/F}$;Lck-Cre* mice were almost completely eliminated, whereas 30% of DP thymocytes in control mice survived (Fig. 3D). To further confirm the effect of *PP6* deficiency on negative selection, we analyzed *PP6*-deficient thymocyte development in a superantigen-mediated deletion model. Superantigen Mtv-8 and Mtv-9 specifically lead to deletion of the Vβ5$^+$ and Vβ11$^+$ TCR clonotypic thymocytes in the presence of the class II MHC molecule I-E^d (33). MHC I-E^d is absent in C57BL/6 mice (H-2$^{b/b}$) but present in BALB/c mice (H-2$^{d/d}$). Enhanced deletion of Vβ5$^+$ and Vβ11$^+$ clones was observed for both CD4 and CD8 SP thymocytes in *PP6$^{F/F}$;Lck-Cre; H-2$^{b/d}$* mice, whereas Vβ8$^+$ thymocytes that did not recognize the superantigen were not affected (Fig. 2E, 2F). This outcome supports the conclusion that negative selection is enhanced in the absence of *PP6*, which may account for the overall reduction of mature CD4 and CD8 SP cells in the thymus of the mutant mice.

Increased IL-17–producing γδ T cells in PP6$^{F/F}$;Lck-Cre mice

In contrast with the severe reduction of αβ T cells, γδ T cells were dramatically increased in the thymus (Fig. 3A) and the periphery

of *PP6$^{F/F}$;Lck-Cre* mice (Fig. 3B and Supplemental Fig. 3A). To determine whether this increase affects all or only subsets of γδ lineages, we examined the repertoire of γδ T cells in the *PP6$^{F/F}$;Lck-Cre* thymus first by quantitative real-time RT-PCR analysis of seven individual Vγ genes. We found that the expression of Vγ5 and Vγ6 fragments increased ~30 and ~50 times, respectively, in the γδ T cells purified from *PP6$^{F/F}$;Lck-Cre* thymus in comparison with those of the control mice (Supplemental Fig. 3B). Vδ1 expression was also found to be increased ~40-fold (Supplemental Fig. 3B). FACS analysis with Vγ-specific Abs revealed that the dramatic increase of γδ T cell numbers in *PP6$^{F/F}$;Lck-Cre* thymus is primarily due to an increase of Vγ6$^+$ cells, even though numbers of Vγ1$^+$ and Vγ5$^+$ cells also increased (Fig. 3C and Supplemental Fig. 3C, 3D). γδ T cells expressing Vγ6, which are normally pairs with Vδ1, represent the major IL-17 producers among γδ lineage T cells and can be identified based on high-level expression of IL-7R and CCR6 (a marker for IL-17–producing T cells) and low-level expression of CD27 (a marker of IFN-γ–producing γδ T cells) (34). Indeed, we found that most *PP6$^{F/F}$;Lck-Cre* γδ T cells were IL-7R^{hi}, CCR6^{hi}, and CD27^{lo} IL-17 producers (Fig. 3D and Supplemental Fig. 3E). Vγ6$^+$ T cells are typically generated in fetal thymus in WT mice (34, 35). However, this population appeared to be continuously increased in *PP6$^{F/F}$;Lck-Cre* mice only after birth (Fig. 3E and Supplemental Fig. 3F). To determine whether the increase of Vγ6$^+$ IL-17–producing γδ T cells is a result of enhanced postnatal development or expansion of fetal-derived cells, we performed an adoptive transfer test using bone marrow donors derived from the *PP6$^{F/F}$;Lck-Cre* mice. Although the mutant donor cells showed defects in αβ lineage development similar to that observed in *PP6$^{F/F}$;Lck-Cre* mice (Supplemental Fig. 3H), they failed to recapitulate the mutant phenotype of *PP6*-deficient γδ T cells (Fig. 3F). Therefore, the increase of γδ T cells in *PP6$^{F/F}$;Lck-Cre* mice is most likely due to continuing expansion of fetal-derived Vγ6$^+$ γδ T cells in the postnatal life. To directly assess the proliferation status of these cells, we pulse-labeled the mice with BrdU. Increased BrdU labeling was observed among both immature (CD24^{hi}) and mature (CD24^{lo}) γδ T cells in *PP6$^{F/F}$;Lck-Cre* mice at the neonatal stage (Fig. 3G). In young adult mice (6–8 wk), there were still a higher percentage of BrdU$^+$ immature γδ T cells, but the proportion of BrdU$^+$ mature γδ T cells was reduced (Fig. 3H). However, the net quantity of BrdU$^+$ mature γδ T cells, which composed the majority of γδ T cells in *PP6$^{F/F}$;Lck-Cre* mice (Supplemental Fig. 3I), was still 35 times more than the controls (Fig. 3I). In addition to the overall increase in cell proliferation, we found that *PP6*-deficient mature γδ T cells were less susceptible to apoptosis (Fig. 3J). Therefore, we concluded that *PP6* deficiency promotes a continuing expansion of pre-existing Vγ6$^+$ γδ T cells in the adult life.

Chronic T cell activation, hyperproliferation, and enhanced apoptosis of effector T cells in PP6*-deficient mice*

To examine functions of *PP6* in peripheral T cells, we switched to the *CD4-Cre* model, in which a significantly higher number of peripheral T cells were found in comparison with the *Lck-Cre* model. The total numbers of splenic CD4$^+$ and CD8$^+$ T cells in *PP6$^{F/F}$;CD4-Cre* mice were ~70 and 42% of the *PP6$^{F/F}$* controls, respectively (Fig. 4A). Naive CD4$^+$ or CD8$^+$ T cells are significantly reduced in *PP6$^{F/F}$;CD4-Cre* mice (Fig. 4B). Most T cells showed activated phenotype based on increased expression of activation markers including CD69 and CD44 (Fig. 4B, 4C). PMA/ionomycin stimulation of ex vivo culture revealed a significant increase in numbers of IFN-γ–producing effector CD4$^+$ or CD8$^+$ cells in *PP6*-deficient splenocytes (Fig. 4D). The same analysis also revealed a small increase in IL-4– or IL-17–producing effector CD4$^+$ cells (Fig. 4E, 4F). Consistent with these effector phenotypes, *PP6*-deficient CD4$^+$ and CD8$^+$ T cells were found highly proliferative based on increased fractions of Ki67$^+$ cells (Fig. 4G). Enhanced proliferation of the effector T cells was further confirmed by CFSE dilution assay of *PP6*-deficient OT-II T cells. Upon adoptive transfer, *PP6*-deficient OT-II T cells underwent faster proliferation than *PP6*-sufficient T cells within 3 d of $OVA_{323–339}$ peptide stimulation (Fig. 4H). These results indicate that *PP6* deficiency promotes T cell activation and proliferation under normal homeostatic conditions, leading to quick depletion of the naive T cell pool.

To further determine the cause of overall reduction of peripheral T cells in *PP6*-deficient mice, we examined whether T cell hyperactivation leads to faster turnover of the effector T cells. Annexin V/7AAD FACS analysis showed a decreased viability of *PP6*-deficient CD4$^+$ and CD8$^+$ T cells in ex vitro culture (Fig. 5A). Adoptive transfer test further demonstrated an intrinsic survival defect of *PP6*-deficient CD4$^+$ and CD8$^+$ T cells (Fig. 5B). The increase in cell death is correlated with an increased loss of mitochondrial membrane potential, increased production of reactive oxygen species, and reduced expression of Bcl-2 (Fig. 5C, 5D). Collectively, these experimental evidences indicate that *PP6* deficiency leads to activation, differentiation, proliferation, and apoptosis of the peripheral T cells in the absence of exogenous TCR signals.

Downregulation of proximal TCR signaling and TCR expression in PP6-deficient T cells

The overall increase in thymocyte positive and negative selections and T cell activation strongly suggest that *PP6* functions as a negative regulator in TCR signaling. To determine how *PP6* modulates TCR signaling events, we first assessed the expression and activation status of proximal TCR signaling molecules in *PP6$^{F/F}$;Lck-Cre* thymocytes. The surface expressions of TCRβ and CD3 were reduced in *PP6*-deficient thymocytes (Fig. 6A). Upon TCR stimulation, the phosphorylations of Zap70, LAT, and LCK proteins were reduced in *PP6*-deficient cells (Fig. 6B). Activation of PLCγ1, which is responsible for the production of the second messenger diacylglycerol and the initiation of Ca^{2+} signaling in T cells, was decreased (Fig. 6B). Consequently, TCR-induced calcium flux was also reduced in these thymocytes (Fig. 6C). The similar results were also obtained for the peripheral T cells of *PP6$^{F/F}$;CD4-Cre* mice (Supplemental Fig. 4A–C, 4E). Thus, the hypoactivation of proximal TCR signaling observed in *PP6*-deficient T cells suggests that *PP6* is unlikely involved in negative regulation of the proximal TCR signaling.

Negative regulation of distal TCR signaling by PP6

TCR signals consist of both membrane-proximal events and multiple distal pathways. To further understand the molecular mechanism(s) by which *PP6* regulates T cell development, we examined the activation of ERK in thymocytes from *PP6$^{F/F}$;Lck-Cre* mice by intracellular staining. The analysis showed that regardless of PMA stimulation, enhanced phosphorylated ERK was detected in both γδ and αβ thymocytes from *PP6*-deficient mice (Supplemental Fig. 4F). Then, we further verified ERK hyperactivation and evaluated the activation status of other distal TCR signaling molecules in *PP6*-deficient thymocytes by Western blot. We found that the phosphorylation levels of ERK, JNK, p38, and AKT were all higher in intensity and retained for a longer duration in *PP6*-deficient thymocytes after PMA/ionomycin (Fig. 7A) or TCR stimulation (Supplemental Fig. 4G). Moreover, the upstream kinases of MAPKs including c-Raf, MEK1/2, MKK4, and MKK3/

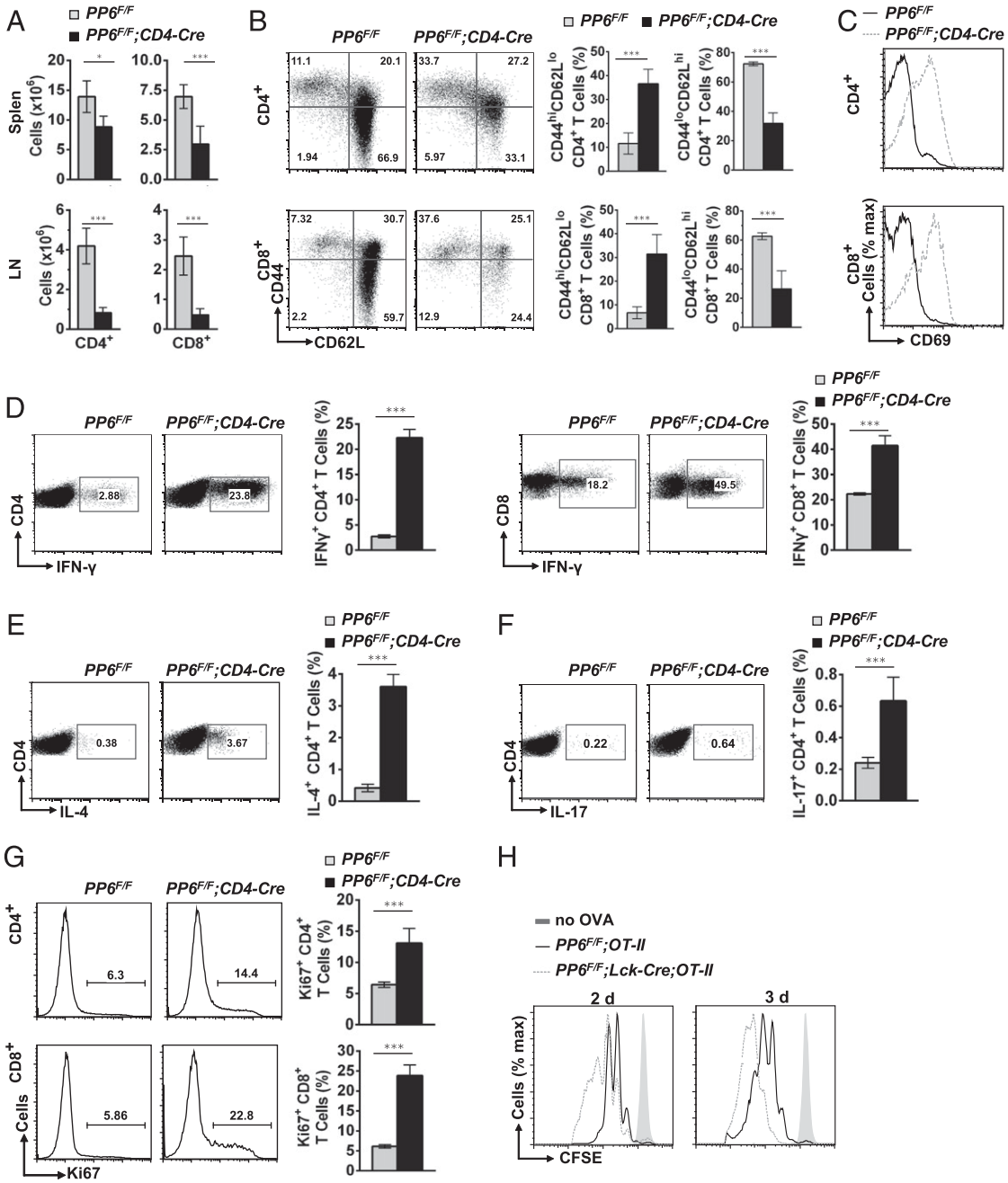

FIGURE 4. Hyperactivation of *PP6*-deficient T cells in the periphery. (**A**) Cellularity of $CD4^+$ and $CD8^+$ lymphocytes from spleen and lymph node (LN) of $PP6^{F/F}$ and $PP6^{F/F}$*;CD4-Cre* mice. $n = 8$ for each genotype. (**B**) Flow cytometry for CD62L and CD44 expression and percentage of $CD44^{hi}CD62L^{lo}$ and $CD44^{lo}CD62L^{hi}$ splenic $CD4^+$ and $CD8^+$ T cells from $PP6^{F/F}$ and $PP6^{F/F}$*;CD4-Cre* mice. $n = 4$ for each genotype. (**C**) CD69 expression on splenic $CD4^+$ and $CD8^+$ T cells from $PP6^{F/F}$ and $PP6^{F/F}$*;CD4-Cre* mice. (**D**–**F**) Flow cytometry and percentage of IFN-γ^+CD4^+ or IFN-γ^+CD8^+ (D), IL-4^+CD4^+ (E), and IL-17^+CD4^+ (F) splenocytes after PMA/ionomycin stimulation for 6 h. (**G**) Intracellular staining of Ki67 in $CD4^+$ and $CD8^+$ splenocytes with indicated genotypes. $n = 3$ for each genotype. (**H**) Purified splenic $CD4^+$ T cells from $PP6^{+/F}$*;OT-II* and $PP6^{F/F}$*;Lck-Cre;OT-II* mice were labeled with CFSE and i.v. transferred into B6.SJL mice. CFSE dilution was analyzed by FACS 2 and 3 d after stimulated with 40 μg $OVA_{323–339}$ peptide per recipient mice. Data shown are representative from three (B–E, H) or two (G) independent experiments. (A, B, and D–G) Data are presented as mean ± SD. $*p < 0.05$, $***p < 0.001$.

6 were also hyperactivated in these cells (Fig. 7B). Similarly, enhanced activation of MAPKs and AKT was observed in the *PP6*-deficient periphery T cells from $PP6^{F/F}$*;CD4-Cre* mice (Supplemental Fig. 4D, 4J), in which the activation of these signals was critical to promote their proliferation and cytokine production (36, 37). These data suggest that hyper and prolonged upregulation of MAPKs and AKT activities may account for enhanced thymocyte positive/negative selection and hyperactivation of T cells in *PP6*-deficient mice.

PP6 has been shown to directly regulate TAK1 and Aurora A (11, 15). TAK1 is essential for the activation of JNK, p38, and NF-κB in T cells (23). Aurora A has been shown to activate AKT (38, 39) and ERK (38–41) in cancer cell lines. TAK1 phosphorylation was markedly reduced in *PP6*-deficient thymocytes after PMA/ionomycin stimulation (Fig. 7C), indicating that hyperactivation of JNK and p38 in *PP6*-deficient T cells is not due to overactivation of TAK1. In contrast with TAK1, Aurora A in *PP6*-deficient T cells was observed to be constitutively active with

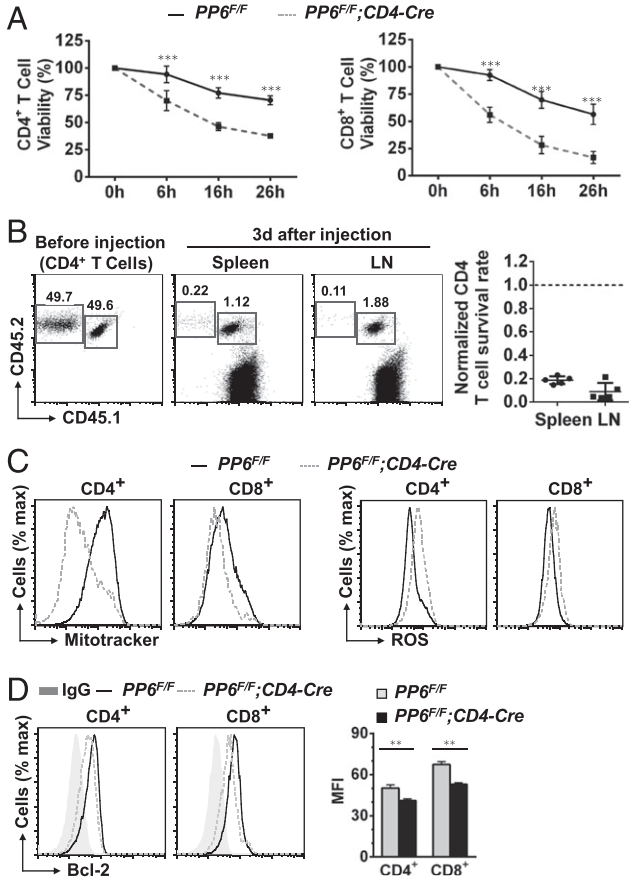

FIGURE 5. Reduced viability of *PP6*-deficient periphery T cells. (**A**) Cell viability of $CD4^+$ and $CD8^+$ splenocytes from $PP6^{F/F}$ and $PP6^{F/F}$;*CD4-Cre* ex vivo cultured for indicated time. Annexin V^-/$7AAD^-$ cells were considered viable. Four pairs of mice were used for each independent experiment. (**B**) Flow cytometry of $CD4^+$ T cells from spleen and lymph node (LN) 3 d after adoptive transfer of splenocytes (with equal number of $CD4^+$ T cells) from $PP6^{F/+}$;$CD45.1.2^+$ and $PP6^{F/F}$;*CD4-Cre*;$CD45.2.2^+$ mice into B6.SJL ($CD45.1.1^+$) recipient mice. Numbers above boxed areas indicate percent cells originated from control and mutant mice. For statistical analysis, viability of *PP6*-deficient cells was normalized to the control (B, *right panels*). $n = 5$ for each genotype. (**C**) FACS analysis of $CD4^+$ and $CD8^+$ T cells from $PP6^{F/F}$ and $PP6^{F/F}$;*CD4-Cre* mice, stained with MitoTracker Green (*left*) or dihydroethidium (*right*). $n = 4$ for each genotype. (**D**) FACS analysis of Bcl-2 intracellular staining and statistical analysis of the mean fluorescent intensity (MFI) for Bcl-2 expression in splenic $CD4^+$ and $CD8^+$ T cells with indicated genotypes. Three pairs of mice were used for each independent experiment. Data shown are representative from two (A, B, and D) and three (C). (A, B, and D) Data are presented as mean ± SD. $^{**}p < 0.01$, $^{***}p < 0.001$.

or without PMA/ionomycin (Fig. 7E) or TCR stimulation (Supplemental Fig. 4H). Thus, PP6 might downregulate distal TCR signals, for example, the ERK and AKT signals, by suppressing Aurora A activity (see *Discussion*).

The NF-κB pathway also plays critical roles in thymocyte selection and T cell activation (42, 43). Constitutive activation of NF-κB activity in thymocytes pushes the most thymocytes into negative selection (32). The phosphorylation of NF-κB (p65) in *PP6*-deficient thymocytes was higher than that in the control with or without TCR stimulation (Supplemental Fig. 4I) and can be further enhanced by PMA/ionomycin stimulation (Fig. 7D), whereas its upstream kinase, IKKβ, was hyperactivated in response to TCR (Supplemental Fig. 4I) or PMA/ionomycin stimulations (Fig. 7D). Our further analysis showed that phosphorylation of IκBα in *PP6*-deficient thymocytes stimulated by PMA/ionomycin was comparable with the control (Fig. 7D), and its degradation in thymocytes could not be efficiently stimulated by TCR engagement (Supplemental Fig. 4I). We also found that IκBε was robustly phosphorylated in the mutant thymocytes after PMA/ionomycin stimulation (Fig. 7D). This result is consistent with the previous report that *PP6* negatively regulated phosphorylation and degradation of IκBε in HeLa cells (14). However, we do not think that *PP6* deficiency–mediated deregulation of IκBε in T cells may contribute much to the developmental defect of *PP6*-deficient T cells (see *Discussion*).

Collectively, these data indicate that *PP6* negatively regulates TCR signaling through modulating multiple pathways distal to the initial TCR signal events. Removal of *PP6* leads TCR-dependent hyperactivation of MAPKs, AKT, and NF-κB pathways, and consequently enhances positive/negative selection and T cell activation.

Discussion

In this article, we present genetic and molecular evidences that *PP6* is critical for the regulation of T cell development and homeostasis. Our data show that *PP6* deficiency results in enhanced positive/negative selection accompanied with a dramatic reduction of αβ thymocytes, an expansion of γδ T cells, and loss of homeostasis of peripheral T cells. Mechanistically, ablation of *PP6* leads to hyperactivation of distal TCR signaling involving MAPKs, AKT, and NF-κB pathways. These findings place PP6 at a major control point of distal TCR signaling.

Although distal TCR signals are markedly increased in *PP6*-deficient cells, the activation of proximal TCR signals are paradoxically decreased and the expressions of TCRβ and CD3 on the surface of *PP6*-deficient thymocytes and peripheral T cells are lower than the control. One possible explanation for this paradoxical phenomenon could be that the cells expressing higher levels of TCR and CD3 are preferentially eliminated by *PP6* deficiency–mediated enhanced negative selection, whereas only those with lower levels of TCR survive. Another explanation could be that hyperactivation of distal TCR signaling in *PP6*-deficient T cells may increase trafficking of TCR–CD3 complexes to lysosomes for degradation because overexpression of constitutive active Lck^{Y505F} was reported to reduce TCR surface expression by this mechanism (44). Currently, we also cannot rule out the possibility that *PP6* positively regulate the activities of proximal TCR molecules. Further studies are needed to test these possibilities.

Positive and negative selection is defined by the ability of TCR to sense relatively weak and overly strong signals, respectively. However, the regulation, particularly negative regulation, of distal TCR signaling cascade in positive and negative selection of thymocytes is not completely known. The test of positive selection using OT-II transgenic TCR demonstrates that *PP6* deficiency enhances positive selection of thymocytes. However, the total number of CD4 SP cells, along with CD8 SP and DP thymocytes, in non-TCR transgenic $PP6^{F/F}$;*Lck-Cre* mice is decreased. This discrepancy suggests that enhanced positive selection applies only to a fraction of developing T cells in *PP6*-deficient thymi, presumably those expressing relatively low-affinity TCR such as OT-II. *PP6*-deficient thymocytes expressing higher-affinity TCR, such as OT-I, may undergo negative selection instead of increased positive selection as observed in our analysis of $PP6^{F/F}$;*Lck-Cre*;*OT-I* mice. Our finding is reminiscent to that observed in thymocytes expressing a constitutively active NF-κB, which is sufficient to push a portion of positively selecting CD4 and CD8 SP thymocytes into pseudonegative selection (32). Our analysis of distal TCR signaling pathways indicates that *PP6* negatively

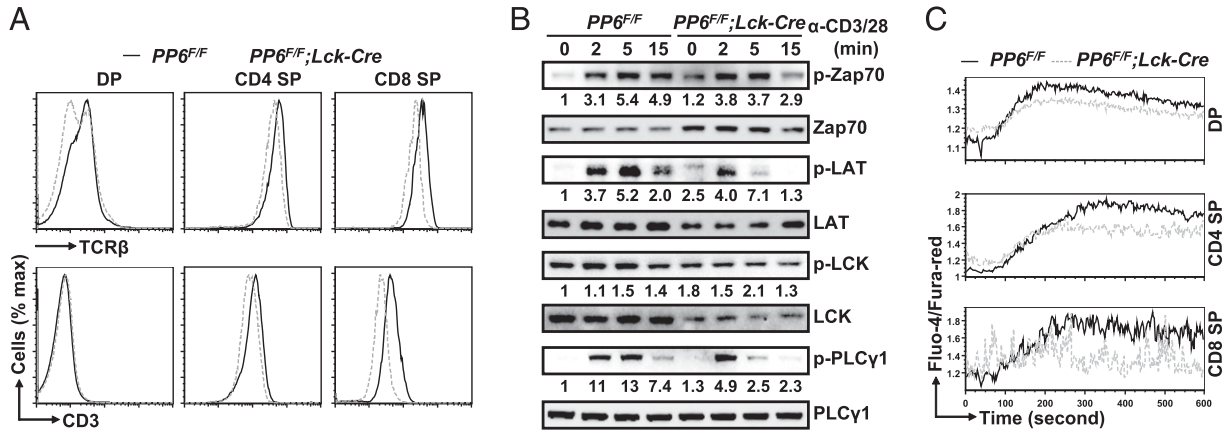

FIGURE 6. Attenuation of proximal TCR signaling in *PP6*-deficient thymocytes. (**A**) Surface expression of TCRβ (*top*) and CD3 (*bottom*) on the DP, CD4 SP, and CD8 SP thymocytes from $PP6^{F/F}$ and $PP6^{F/F}$;*Lck-Cre* mice. (**B**) Immunoblot analysis for the activation (phosphorylation) of Zap70, LAT, LCK, and PLCγ1 in thymocytes from $PP6^{F/F}$ and $PP6^{F/F}$;*Lck-Cre* mice. Total thymocytes were stimulated with anti-CD3/CD28 mAbs for the indicated time. Total Zap70, LAT, LCK, and PLCγ1 were served as loading controls. Numbers below lanes represent band intensity relative to the respective total proteins. (**C**) Flow cytometry for calcium flux in DP, CD4 SP, and CD8 SP thymocytes from $PP6^{F/F}$ and $PP6^{F/F}$;*Lck-Cre* mice. The cells were stained with calcium indicators Fluo-4 and Fura Red followed by stimulation with anti-CD3/CD28 mAbs. Data are representative of four (A), three (B), and two (C) independent experiments.

regulates multiple pathways known to be involved in either positive (e.g., ERK pathway) or negative (e.g., NF-κB and JNK pathways) selection. Thus, the TCR distal signaling pathways responsible for both positive and negative selection are attenuated by the PP6 phosphatase.

Our study has shown that the number of γδ T cells dramatically increased in both thymus and peripheral lymphoid organs of $PP6^{F/F}$;*Lck-Cre* mice. However, the expansion of γδ T cells was mainly restricted to the IL-17–producing $V\gamma6^{+}$ γδ T cells, with mild or no increase of other Vγ subpopulations. One possible explanation could

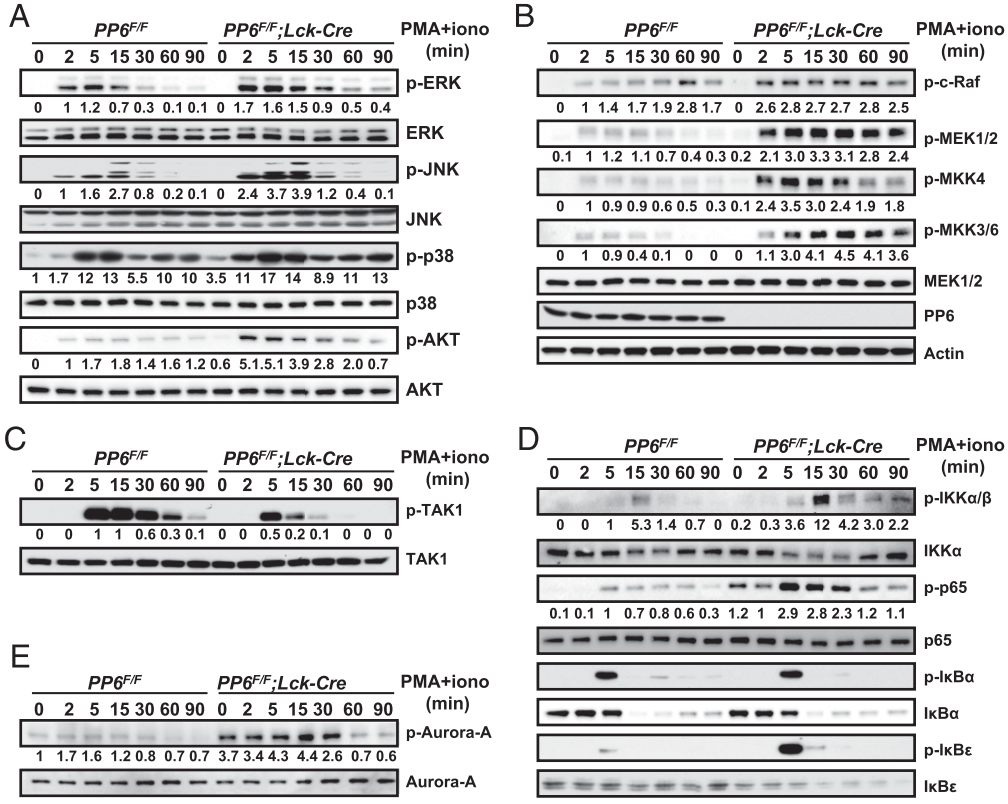

FIGURE 7. Hyperactivation of distal TCR signaling in *PP6*-deficient thymocytes. (**A** and **B**) Immunoblot analysis for the activation of MAPKs, AKT (A), and their upstream molecules including c-Raf, and MAP2Ks (MEK1/2, MKK4 and MKK3/6) (B) in PMA/ionomycin-stimulated thymocytes from $PP6^{F/F}$ and $PP6^{F/F}$;*Lck-Cre* mice using indicated Abs. Total thymocytes were stimulated with PMA/ionomycin for indicated time. Actin was served as a loading control. (**C** and **E**) Immunoblot analysis for the activation of TAK1 (C) and Aurora A (E) with the same lysates in (A) using indicated Abs. Total TAK1 or Aurora A was served as loading controls. (**D**) Immunoblot analysis for the activation of NF-κB signaling pathway with the same lysates in (A) using indicated Abs. Numbers below lanes represent band intensity relative to the respective total proteins. Data are representative of four (A) and three (B–E) independent experiments.

be that *PP6* deficiency might extend the window of using Vγ6 gene fragments beyond embryonic stage. However, our finding that *PP6*-deficient γδ T cells were not increased in bone marrow recipient mice argues strongly against this possibility. The second possible explanation is that the differential effects of *PP6* deficiency on each Vγ subset might depend on their corresponding affinities to selecting ligands. Vγ1Vδ6.3 is thought to be a high-affinity TCR (45), whereas Vγ6Vδ1 may be an intermediate-affinity TCR, because $V\gamma6^+$ T cells, which composed a majority of γδ T cells in *PP6*$^{F/F}$*; Lck-Cre* mice, expressed a lower level of CD5 (Supplemental Fig. 3J). Correspondingly, the number of $V\gamma1^+$ T cells was only slightly (1.5-fold) increased, and $V\gamma6^+$ T cells upsurged >100-fold in *PP6*$^{F/F}$*; Lck-Cre* mice (Fig. 3C). Thus, we postulate that *PP6* deficiency–mediated hyperactivation of distal TCR signaling (e.g., ERK) may have greater impact on IL-17–producing $V\gamma6^+$ γδ T cells than other γδ T cells that possess different affinity of γδ TCR. Our postulation is consistent with the previous report that stronger TCR signal promotes the development of γδ T cells in Vγ6Vδ1 TCR transgenic mice (46). In contrast, the reduced Zap70 activity in the SKG mouse (47) or attenuated ERK activation in *RasGRP1*$^{-/-}$ mice (48) results in decreased proportion of IL-17–producing γδ T cells and an increased proportion of IFN-γ–producing γδ T cells.

Our study shows that multiple distal TCR signal pathways such as MAPKs, AKT, and NF-κB pathways were all hyperactivated in *PP6*-deficient T cells. We have also found that two known direct targets, Aurora A kinase and IκBε, of PP6 phosphatase are hyperphosphorylated in these cells. Although the *IκBε* null mutation results in dramatic hyperactivation of NF-κB and can augment the T cell developmental defect of *IκBα*-null mutant mice (49), the *IκBε* null mice do not display any abnormality of T cell population except for a 50% reduction of the DN3 ($CD44^-$ $CD25^+$) T cell subspecies (50). The population and cell number of αβ T cells at DN stage are not affected in our *PP6*$^{F/F}$*;Lck-Cre* mice. Therefore, we do not think that robust phosphorylation and sped-up degradation in *PP6*-deficient T cells contribute much to the altered behavior of *PP6*-deficient T cells. Regarding Aurora A, we think that its overactivation may account for part of the hyperactivation of distal TCR signaling resulting from *PP6* deficiency. However, due to the extremely low viability of ex vivo cultured *PP6*-deficient T cells, we failed to use ex vivo cultured *PP6*-deficient T cells to test whether reduction or inhibition of Aurora A could rescue or partially rescue *PP6* deficiency–mediated mutant phenotypes. Further evaluation of T cell development and status of distal TCR signal in *PP6* and *Aurka* double-knockout mice will help to uncover the role of PP6-Aurora A signaling in the regulation of T cell development and homeostasis. Furthermore, additional targets of PP6, particularly those involved in regulating the MAPKs, still remain to be defined. Results presented in this study of *PP6*-deficient mouse model reveal that *PP6* must be a major negative regulator involved in modulating multiple TCR distal pathways. This negative regulator is critical to balance the positive TCR signals, ensuring generation and maintenance of a stable population of naive T cells.

Acknowledgments

We thank Dr. Robert E. Tigelaar (Yale University, New Haven, CT) for providing TCR Vγ6 mAbs. We thank Dr. Xuetao Cao (Second Military Medical University, Shanghai, China) for kindly providing OT-II and OT-I mice. We also thank Dr. Xiaohui Wu for scientific discussion and Xiaofeng Tao for English editing.

Disclosures

The authors have no financial conflicts of interest.

References

1. Brownlie, R. J., and R. Zamoyska. 2013. T cell receptor signalling networks: branched, diversified and bounded. *Nat. Rev. Immunol.* 13: 257–269.
2. Palmer, E. 2003. Negative selection—clearing out the bad apples from the T-cell repertoire. *Nat. Rev. Immunol.* 3: 383–391.
3. Rothenberg, E. V., J. E. Moore, and M. A. Yui. 2008. Launching the T-cell-lineage developmental programme. *Nat. Rev. Immunol.* 8: 9–21.
4. Sprent, J., and C. D. Surh. 2011. Normal T cell homeostasis: the conversion of naive cells into memory-phenotype cells. *Nat. Immunol.* 12: 478–484.
5. Rhee, I., and A. Veillette. 2012. Protein tyrosine phosphatases in lymphocyte activation and autoimmunity. *Nat. Immunol.* 13: 439–447.
6. Huang, C. Y., and T. H. Tan. 2012. DUSPs, to MAP kinases and beyond. *Cell Biosci.* 2: 24.
7. Shi, Y. 2009. Serine/threonine phosphatases: mechanism through structure. *Cell* 139: 468–484.
8. Brechmann, M., T. Mock, D. Nickles, M. Kiessling, N. Weit, R. Breuer, W. Müller, G. Wabnitz, F. Frey, J. P. Nicolay, et al. 2012. A PP4 holoenzyme balances physiological and oncogenic nuclear factor-kappa B signaling in T lymphocytes. *Immunity* 37: 697–708.
9. Shui, J. W., M. C. Hu, and T. H. Tan. 2007. Conditional knockout mice reveal an essential role of protein phosphatase 4 in thymocyte development and pre-T-cell receptor signaling. *Mol. Cell. Biol.* 27: 79–91.
10. Stefansson, B., T. Ohama, A. E. Daugherty, and D. L. Brautigan. 2008. Protein phosphatase 6 regulatory subunits composed of ankyrin repeat domains. *Biochemistry* 47: 1442–1451.
11. Hammond, D., K. Zeng, A. Espert, R. N. Bastos, R. D. Baron, U. Gruneberg, and F. A. Barr. 2013. Melanoma-associated mutations in protein phosphatase 6 cause chromosome instability and DNA damage owing to dysregulated Aurora-A. *J. Cell Sci.* 126: 3429–3440.
12. Zhong, J., J. Liao, X. Liu, P. Wang, J. Liu, W. Hou, B. Zhu, L. Yao, J. Wang, J. Li, et al. 2011. Protein phosphatase PP6 is required for homology-directed repair of DNA double-strand breaks. *Cell Cycle* 10: 1411–1419.
13. Hosing, A. S., N. C. K. Valerie, J. Dziegielewski, D. L. Brautigan, and J. M. Larner. 2012. PP6 regulatory subunit R1 is bidentate anchor for targeting protein phosphatase-6 to DNA-dependent protein kinase. *J. Biol. Chem.* 287: 9230–9239.
14. Stefansson, B., and D. L. Brautigan. 2006. Protein phosphatase 6 subunit with conserved Sit4-associated protein domain targets IkappaBepsilon. *J. Biol. Chem.* 281: 22624–22634.
15. Kajino, T., H. Ren, S. Iemura, T. Natsume, B. Stefansson, D. L. Brautigan, K. Matsumoto, and J. Ninomiya-Tsuji. 2006. Protein phosphatase 6 down-regulates TAK1 kinase activation in the IL-1 signaling pathway. *J. Biol. Chem.* 281: 39891–39896.
16. Couzens, A. L., J. D. Knight, M. J. Kean, G. Teo, A. Weiss, W. H. Dunham, Z. Y. Lin, R. D. Bagshaw, F. Sicheri, T. Pawson, et al. 2013. Protein interaction network of the mammalian Hippo pathway reveals mechanisms of kinase-phosphatase interactions. *Sci. Signal.* 6: rs15.
17. Pan, L., J. Hanrahan, J. Li, L. P. Hale, and Y. Zhuang. 2002. An analysis of T cell intrinsic roles of E2A by conditional gene disruption in the thymus. *J. Immunol.* 168: 3923–3932.
18. Wolfer, A., A. Wilson, M. Nemir, H. R. MacDonald, and F. Radtke. 2002. Inactivation of Notch1 impairs VDJbeta rearrangement and allows pre-TCR-independent survival of early alpha beta lineage thymocytes. *Immunity* 16: 869–879.
19. Sun, L., X. Wu, M. Han, T. Xu, and Y. Zhuang. 2008. A mitotic recombination system for mouse chromosome 17. *Proc. Natl. Acad. Sci. USA* 105: 4237–4241.
20. Du, X., H. Shi, J. Li, Y. Dong, J. Liang, J. Ye, S. Kong, S. Zhang, T. Zhong, Z. Yuan, et al. 2014. Mst1/Mst2 regulate development and function of regulatory T cells through modulation of Foxo1/Foxo3 stability in autoimmune disease. *J. Immunol.* 192: 1525–1535.
21. Dong, Y., X. Du, J. Ye, M. Han, T. Xu, Y. Zhuang, and W. Tao. 2009. A cell-intrinsic role for Mst1 in regulating thymocyte egress. *J. Immunol.* 183: 3865–3872.
22. Roark, C. L., M. K. Aydintug, J. Lewis, X. Yin, M. Lahn, Y. S. Hahn, W. K. Born, R. E. Tigelaar, and R. L. O'Brien. 2004. Subset-specific, uniform activation among V gamma 6/V delta 1+ gamma delta T cells elicited by inflammation. *J. Leukoc. Biol.* 75: 68–75.
23. Wan, Y. Y., H. Chi, M. Xie, M. D. Schneider, and R. A. Flavell. 2006. The kinase TAK1 integrates antigen and cytokine receptor signaling for T cell development, survival and function. *Nat. Immunol.* 7: 851–858.
24. Kong, S., X. Du, C. Peng, Y. Wu, H. Li, X. Jin, L. Hou, K. Deng, T. Xu, and W. Tao. 2013. Dlic1 deficiency impairs ciliogenesis of photoreceptors by destabilizing dynein. *Cell Res.* 23: 835–850.
25. Peng, C., J. Ye, S. Yan, S. Kong, Y. Shen, C. Li, Q. Li, Y. Zheng, K. Deng, T. Xu, and W. Tao. 2012. Ablation of vacuole protein sorting 18 (Vps18) gene leads to neurodegeneration and impaired neuronal migration by disrupting multiple vesicle transport pathways to lysosomes. *J. Biol. Chem.* 287: 32861–32873.
26. Azzam, H. S., A. Grinberg, K. Lui, H. Shen, E. W. Shores, and P. E. Love. 1998. CD5 expression is developmentally regulated by T cell receptor (TCR) signals and TCR avidity. *J. Exp. Med.* 188: 2301–2311.
27. Sancho, D., M. Gómez, and F. Sánchez-Madrid. 2005. CD69 is an immunoregulatory molecule induced following activation. *Trends Immunol.* 26: 136–140.
28. Crispe, I. N., and M. J. Bevan. 1987. Expression and functional significance of the J11d marker on mouse thymocytes. *J. Immunol.* 138: 2013–2018.
29. Barnden, M. J., J. Allison, W. R. Heath, and F. R. Carbone. 1998. Defective TCR expression in transgenic mice constructed using cDNA-based alpha- and beta-

chain genes under the control of heterologous regulatory elements. *Immunol. Cell Biol.* 76: 34–40.
30. Hogquist, K. A., S. C. Jameson, W. R. Heath, J. L. Howard, M. J. Bevan, and F. R. Carbone. 1994. T cell receptor antagonist peptides induce positive selection. *Cell* 76: 17–27.
31. Lundberg, K., W. Heath, F. Köntgen, F. R. Carbone, and K. Shortman. 1995. Intermediate steps in positive selection: differentiation of CD4+8int TCRint thymocytes into CD4-8+TCRhi thymocytes. *J. Exp. Med.* 181: 1643–1651.
32. Jimi, E., I. Strickland, R. E. Voll, M. Long, and S. Ghosh. 2008. Differential role of the transcription factor NF-kappaB in selection and survival of CD4+ and CD8+ thymocytes. *Immunity* 29: 523–537.
33. Simpson, E. 1993. T cell repertoire selection by mouse mammary tumour viruses. *Eur. J. Immunogenet.* 20: 137–149.
34. Bonneville, M., R. L. O'Brien, and W. K. Born. 2010. Gammadelta T cell effector functions: a blend of innate programming and acquired plasticity. *Nat. Rev. Immunol.* 10: 467–478.
35. Shibata, K., H. Yamada, R. Nakamura, X. Sun, M. Itsumi, and Y. Yoshikai. 2008. Identification of CD25+ gamma delta T cells as fetal thymus-derived naturally occurring IL-17 producers. *J. Immunol.* 181: 5940–5947.
36. Dong, C., R. J. Davis, and R. A. Flavell. 2002. MAP kinases in the immune response. *Annu. Rev. Immunol.* 20: 55–72.
37. Kane, L. P., and A. Weiss. 2003. The PI-3 kinase/Akt pathway and T cell activation: pleiotropic pathways downstream of PIP3. *Immunol. Rev.* 192: 7–20.
38. Tseng, Y. S., J. C. Lee, C. Y. Huang, and H. S. Liu. 2009. Aurora-A overexpression enhances cell-aggregation of Ha-ras transformants through the MEK/ERK signaling pathway. *BMC Cancer* 9: 435.
39. Zeng, K., R. N. Bastos, F. A. Barr, and U. Gruneberg. 2010. Protein phosphatase 6 regulates mitotic spindle formation by controlling the T-loop phosphorylation state of Aurora A bound to its activator TPX2. *J. Cell Biol.* 191: 1315–1332.
40. Wan, X. B., Z. J. Long, M. Yan, J. Xu, L. P. Xia, L. Liu, Y. Zhao, X. F. Huang, X. R. Wang, X. F. Zhu, et al. 2008. Inhibition of Aurora-A suppresses epithelial-mesenchymal transition and invasion by downregulating MAPK in nasopharyngeal carcinoma cells. *Carcinogenesis* 29: 1930–1937.
41. Li, Y., W. Zhou, L. Wei, J. Jin, K. Tang, C. Li, B. T. Teh, and X. Chen. 2012. The effect of Aurora kinases on cell proliferation, cell cycle regulation and metastasis in renal cell carcinoma. *Int. J. Oncol.* 41: 2139–2149.
42. Gerondakis, S., T. S. Fulford, N. L. Messina, and R. J. Grumont. 2014. NF-κB control of T cell development. *Nat. Immunol.* 15: 15–25.
43. Bonizzi, G., and M. Karin. 2004. The two NF-kappaB activation pathways and their role in innate and adaptive immunity. *Trends Immunol.* 25: 280–288.
44. Sohn, S. J., K. A. Forbush, X. C. Pan, and R. M. Perlmutter. 2001. Activated p56lck directs maturation of both CD4 and CD8 single-positive thymocytes. *J. Immunol.* 166: 2209–2217.
45. Lauritsen, J. P. H., G. W. Wong, S.-Y. Lee, J. M. Lefebvre, M. Ciofani, M. Rhodes, D. J. Kappes, J. C. Zúñiga-Pflücker, and D. L. Wiest. 2009. Marked induction of the helix-loop-helix protein Id3 promotes the gammadelta T cell fate and renders their functional maturation Notch independent. *Immunity* 31: 565–575.
46. Hayes, S. M., L. Li, and P. E. Love. 2005. TCR signal strength influences alphabeta/gammadelta lineage fate. *Immunity* 22: 583–593.
47. Wencker, M., G. Turchinovich, R. Di Marco Barros, L. Deban, A. Jandke, A. Cope, and A. C. Hayday. 2014. Innate-like T cells straddle innate and adaptive immunity by altering antigen-receptor responsiveness. *Nat. Immunol.* 15: 80–87.
48. Chen, Y., X. Ci, B. Gorentla, S. A. Sullivan, J. C. Stone, W. Zhang, P. Pereira, J. Lu, and X. P. Zhong. 2012. Differential requirement of RasGRP1 for γδ T cell development and activation. *J. Immunol.* 189: 61–71.
49. Goudeau, B., F. Huetz, S. Samson, J. P. Di Santo, A. Cumano, A. Beg, A. Israël, and S. Mémet. 2003. IkappaBalpha/IkappaBepsilon deficiency reveals that a critical NF-kappaB dosage is required for lymphocyte survival. *Proc. Natl. Acad. Sci. USA* 100: 15800–15805.
50. Mémet, S., D. Laouini, J. C. Epinat, S. T. Whiteside, B. Goudeau, D. Philpott, S. Kayal, P. J. Sansonetti, P. Berche, J. Kanellopoulos, and A. Israël. 1999. IkappaBepsilon-deficient mice: reduction of one T cell precursor subspecies and enhanced Ig isotype switching and cytokine synthesis. *J. Immunol.* 163: 5994–6005.